Diseño y simulación de un control tolerante a fallas para un panel fotovoltaico.

Mise Pillo, Víctor Hugo y Mosquera Morales, Edison Adrián

Departamento de Eléctrica y Electrónica

Carrera de Ingeniería en Electrónica e Instrumentación

Artículo académico, previo a la obtención del título de Ingeniería en Electrónica e Instrumentación

Dra. Proaño Llanos, Jacqueline del Rosario

16 de agosto del 2023

Latacunga

Fault Identification System Internally Affecting Photovoltaic Panels Using Artificial Intelligence

Victor Mise
Universidad de las Fuerzas Armadas ESPE
Sangolquí-Ecuador
vhmise@espe.edu.ec

Edison Mosquera
Universidad de las Fuerzas Armadas ESPE
Sangolquí-Ecuador
eamosquera@espe.edu.ec

Jacqueline Llanos
Universidad de las Fuerzas Armadas ESPE
Sangolquí-Ecuador
jdllanos1@espe.edu.ec

Ismael Minchala
Tecnológico de Monterrey
Monterrey-Mexico
ismael.minchala@tec.mx

Franklin Silva
Universidad de las Fuerzas Armadas ESPE
Sangolquí-Ecuador
fmsilva@espe.edu.ec

***Abstract*—This research presents the design and simulation of a neural network-based fault identification system for a photovoltaic panel. The system allows detecting mismatch and degradation faults caused by humidity, which are equivalent to the increase or decrease of the internal series resistance of the panel respectively, thus preventing damages that could limit its performance and lifetime. Mismatch failures are caused by the occurrence of hot spots, while panel exposure in humid environments causes failures due to moisture degradation. A photovoltaic panel is modeled using the parameters provided by its manufacturer. A series resistance estimator based on the recursive least square's method with a forgetting factor and upper and lower confidence intervals is proposed. Fault identification is performed using a multilayer perceptron neural network with supervised training. Inputs to the network are irradiance and estimated series resistance value. Outputs are: normal operation, failure due to mismatch and failure due to moisture degradation. The estimator is evaluated for various scenarios, including normal and failures operation. In addition, it is subjected to different solar irradiance profiles based on real data. The estimator demonstrates good performance, correctly identifying all evaluated operating points.**

Keywords—Panel failures, neural networks, recursive least squares with forgetting factor, photovoltaic panel.

I. INTRODUCTION

Technological, economic development of countries and population growth are part of the main reasons for high energy consumption rates [1]. The of annual (carbon dioxide) emissions from fossil fuel combustion are significant factors contributing to global climate change [2]. In the quest for clean energy sources, solar energy is one of the best options for reducing pollution and environmental impact. The future competitiveness of solar energy is driven by countries that support the development of new technologies and research aimed at reducing manufacturing costs. However, factors such as the nature of solar energy, geographical location, and changes in weather conditions can limit the implementation of systems that harness large amounts of solar energy [3].

Despite the limitations, devices have been developed using photovoltaic technology, which converts sunlight irradiance into electricity through the photovoltaic effect [4]. However, this does not imply that PV photovoltaic panels are immune to failures; on the contrary, these commonly occur in their electrical components [5]. PV panels are susceptible to failure due to various common factors, such as humidity, deterioration of internal electrical components, connection breakages, and even human errors [6]. Additionally, PV can experience failures caused by natural conditions, such as shading. Shading prevents the proper delivery of power due to low irradiance levels reaching the panel. These losses can be reduced by using bypass diodes or changing the panel interconnection [7].

In the search for methods to detect and identify faults in photovoltaic energy, the implementation of Neural Networks (NN) is one of the most widely used methods today as it is based on information processing similar to the human brain [8]. This technique relies on numerical weights that adapt to the training type and the number of neurons defined in each layer. There are various types of artificial neural networks, such as Multilayer Perceptron (MLP), which uses non-linear activation functions, and Recursive Neural Networks (RNN), which leverage time series data for deep learning purposes [9].

The identification of faults caused by increases in series resistance is analyzed through a method proposed in [10], which is based on measuring the slope of the current – voltage (I-V) curve at a fixed distance from the short-circuit current. In [11], a method is employed that detects PV degradation based on the increase in series resistance value by analyzing the error in predicting the position at the maximum power point. In [12], parameter estimation of the photovoltaic panel is performed based on a pattern search optimization algorithm as a tool to diagnose possible faults affecting its performance. However, the aforementioned works use artificial intelligence methods or estimation techniques to detect variations caused by a fault in the panel, but they do not define the specific fault and its effects on the panel. This is where the importance lies in identifying specific faults in internal components of the PV that can cause a decrease in its performance and reduce its lifespan.

This research proposes a fault identification model for a PV, the analyzed faults include mismatch and moisture degradation, all of which can affect the performance of the PV. These faults directly cause internal damage to the series resistance R_s of the cells that make up the PV. When failures occur such as: mismatch produce an increase in R_s, while if there is a reduction in the value of it is usually caused by moisture degradation failure [13]. The fault identification model is implemented using a multi-layer perceptron neural network, it is trained based on the value of R_s and various irradiance levels to determine three operational modes at its output, the first mode represents normal operation (NOP), the

second mode represents “Fault 1” due to mismatch, and the third mode represents “Fault 2” caused by moisture degradation, these faults occur when the value of the series resistance increases or decreases, respectively. The fault identification model relies on the value of R_s, which is difficult to measure directly as it is an internal parameter, therefore, this research also proposes an R_s estimator model called R_s, the R_s model is developed using the recursive least squares method in short time intervals, with a 95% confidence interval around the estimated value. This ensures that the estimated $\hat{R}_s$ value falls within a confidence range, minimizing confusion regarding estimation errors and panel faults. The models are evaluated under various radiation scenarios in a simulator (Matlab/Simulink) for their reliability and extensive range of tools.

The main contributions of this research are the following: i) To present a failure identifier in PV systems to prevent damage and extend their useful life, guaranteeing the safety of components susceptible to failure. ii) To provide an alternative to avoid the replacement of panels that present deficiency in their performance caused by misalignment failures and degradation due to humidity. iii) To reduce repair or replacement costs of panels through early detection of failures.

II. Photovoltaic Panel Description and Modeling

In this research a PV operation fault identification model is proposed, the proposal is based on the training of a multilayer perceptron neural network. In order to obtain the data for the training of the PV fault identifier model, a simulated PV model is designed as shown in Fig. 1, which includes a PV with manufacturer's characteristics, a Boost topology DC/DC converter controlled by a MPPT algorithm based on the perturb and observe (P&O) method, a local load that can take different values. The PV inputs are the irradiance G, and temperature T_o, in addition, the PV has a series resistance R_s given by the manufacturer, if R_s changes to a high value, "Fault 1" of mismatch type occurs, while a minimum value of R_s causes "Fault 2", caused by humidity degradation. Where I_{pv} and V_{pv} is the PV current and voltage, the elements that make up the Boost converter are: the L_{pv} coil, the C_{pv} capacitor, the mosfet that receives the PWM G_1 trigger signal and the DC capacitor (C_{DC}).

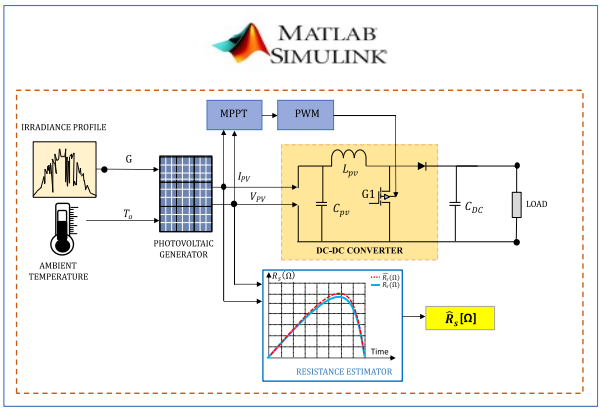

Fig. 1. Schematic of the process of identifying faults in a photovoltaic panel.

The PV model should be considered reliable and adaptable for predicting the power generated by series/parallel connected PV cells. The PV is based on a single diode PV cell model comprising a single current source with an antiparallel diode, a parallel shunt resistor and a series resistor R_s, as shown R_{sh} in Fig. 2.

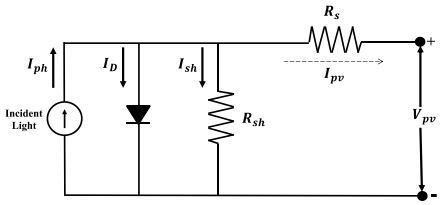

Fig. 2. Model of an equivalent PV cell.

To obtain the current of the photovoltaic cell, it is necessary to apply Kirchhoff’s current law to the model of the single-diode photovoltaic cell. Applying this law yields the equation for the current of the photovoltaic panel as presented in (1). [6]

$$I_{pv} = I_{ph} N_p - I_D - I_{sh} \tag{1}$$

Where the photocurrent is represented as I_{ph}, it occurs when the photovoltaic cell is exposed to incident sunlight. This current is linearly modified relative to a specific temperature and solar irradiance. Additionally, one must consider the number of cells in parallel N_p, the current of the antiparallel diode I_D, and the current of the shunt resistance I_{sh}. In Equation (2), the current of the shunt resistance I_{sh} is obtained using the method of Kirchhoff’s current laws. [6]

$$I_{sh} = \frac{V_{pv} + I_{pv} R_s}{R_{sh}} \tag{2}$$

In Equation (1), the equations (2) are substituted to obtain the value of the overall photovoltaic panel current, as expressed in Equation (3).

$$I_{pv} = I_{ph} N_p - I_D - \left(\frac{V_{pv} + I_{pv} R_s}{R_{sh}} \right) \tag{3}$$

III. Photovoltaic Panel Failures

A failure is interpreted as an event that reduces the efficiency of the system, and they are not eliminated without a study of the problem. One of the main causes of PV underperformance is construction defects. Any instability in the magnitude of the component causes power drop degradation [14]. PV e systems are prone to experience physical faults caused by the insulation of the wires in the various component strings, resulting in open circuit faults in the PV generators. Line faults are caused by low impedance current shifting in a PV array. There is a close resemblance between line faults and ground faults, but the low impedance path is from the current inducing conductor to ground. A summary of the faults that PV systems can experience, along with their causes and the effects to which they are typically exposed, is presented in [15].

A. Mismatch Failure

Mismatch faults are produced when there is a variation in the electrical values of the photovoltaic module compared to

its original state. This occurs when the cells are exposed to shade, causing hot spots and a decrease in dissipated power affecting the internal components, such as changes in the value of R_s [16].

B. *Potting Failures and Moisture Degradation*

Encapsulation failure and degradation occur when solar panels are exposed to hot and humid environments, as well as when they are subjected to increased salts, contaminants, or external agents. Encapsulation failure, specifically delamination, causes power loss, and therefore, degradation leads to wear, simulating a reduction in R_s [17].

IV. Proposed PV Fault Identification System

Once the types of faults have been studied and the faults to be identified in this case have been selected: mismatch faults and degradation due to moisture. The research work proposes a fault identification system in a PV based on neural networks. The implementation of the proposal is shown in Fig 3, where the top part (gray color) presents the photovoltaic system, models the panel, and designs the MPPT controller for the Boost DC/DC converter as described in section II. It is important to highlight that as a technical data of the PV, the value of R_s is available, which increases or decreases depending on the type of fault it presents. This resistance is inherent in the real-life system and is not measurable. For this reason, an estimator of the series resistance is proposed as shown in Fig 3 (green color), the estimator is based on the recursive least squares method with a forgetting factor described in section IV- (A). The inputs of the estimator are V_{pv} and I_{pv}, and the manufacturer's value of R_s, and the output obtained is $\hat{R}_s$ within confidence intervals, to ensure that there is no confusion between estimation error and a fault. The fault identification system shown in Fig 3 (blue color) uses an MLP neural network with two inputs: the radiation G measured inline and $\hat{R}_s$, to obtain as output: NOP, Fault 1 (mismatch), or Fault 2 (degradation due to humidity). This allows the neural network to learn and identify when a fault occurs, resulting in a power change at the PV output, without confusing this change with irradiance variations. The design of the neural network is presented in section IV- (D).

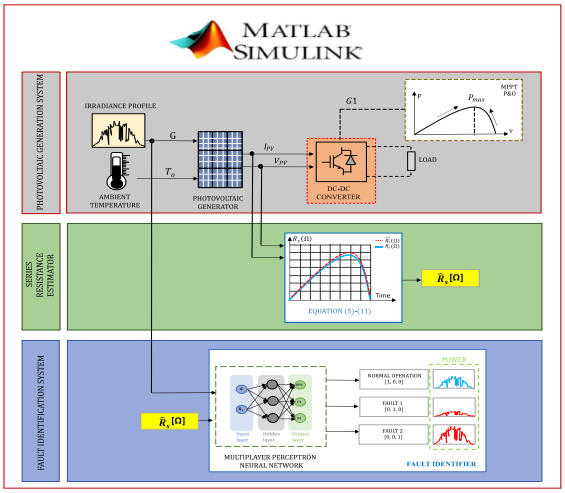

Fig 3. Stages of the failure detection process in a PV.

A. *Proposed Series Resistance Estimator* $(\hat{R}_s)$

This section presents the design of the $\hat{R}_s$ estimator that corresponds to the input of the fault identification model, because R_s is an internal resistance of the panel without access to measurement, under normal conditions its value is maintained at the value specified by the manufacturer. To estimate the value, two stages are considered: the first estimation is by means of the recursive least squares method with forgetting factor (FFRLS), and the second, the application of confidence intervals that guarantees that the estimated values are in a reliability range of 95%.

B. *Technique-Based Estimator (FFRLS)*

The real-time recursive least squares (RLS) technique takes care of the reduction of modeling errors. In addition, the RLS method ensures that the estimated variables resemble the actual values. The PV variables are constantly modified, when the value of T_0 and G changes. The advantage of this technique is shorter measurement times. It is necessary to obtain several parameters for this estimation such as the value of the estimated current $\hat{I}_{pv}(x)$ which is obtained by applying OHM's Law described in (4), where: $V_{pv}(x)$ is the vector of the PV voltage values, $\hat{R}_s(x)$ is the vector of the initial estimation data of $R_s(x)$ to this value is added 0.01 to prevent noise in the data[18].

$$\hat{I}_{pv}(x) = \frac{V_{pv}(x)}{\hat{R}_s(x) + 0.01} \tag{4}$$

In order to achieve accurate estimation, predictions are made in real-time. The Kalman filter is deduced as an RLS estimation to modify and improve the estimated value. To obtain the Kalman gain $K(x)$, in (5) is used, where P_0 represents the initial parameter of the covariance matrix that encompasses the problem data in the estimation process.

$$K(x) = \frac{P_0}{P_0 + 1} \tag{5}$$

To improve the estimated value obtained with RLS, a forgetting factor called (λ) is applied, which updates the estimated data over time and whose value must be between $(0 < \lambda \leq 1)$. If $\lambda < 1$, in other words, the correct value for λ is obtained through trial and error [13]. The current parameter of the covariance matrix P is calculated using in (6), where a value of 0.98 is considered for λ.

$$P = \left(\frac{1}{\lambda}\right) \cdot \left(P_0 - \left(K(x) \cdot P_0\right)\right) \tag{6}$$

The data of the estimator $\hat{R}_s$ are contained within a vector of variables obtained in (7), where $\hat{R}_s(x-1)$ represents the previous value of the estimation of R_s, $K(x)$ is the Kalman gain, $e(x)$ is the residual error, and x represents the number of samples [19].

$$\hat{R}_s(x) = \hat{R}_s(x-1) + K(x)\left[e(x)\right] \tag{7}$$

$$e(x) = I_{pv}(x) - \hat{I}_{pv}(x) \tag{8}$$

In equation (8), the residual error produced by the recursive least square's method is shown. It represents the

difference between the current $I_{pv}(x)$ and the estimated current $\hat{I}_{pv}(x)$.

C. Confidence Interval

This section describes the method used for calculating confidence intervals of the estimated resistance. This allows determining if $\hat{R}_s$ is within normal operating ranges. When the sample values are small, it is necessary to use the student's t-distribution to obtain correct confidence intervals and hypothesis testing. For the application of the t-distribution, the calculation of the standard deviation S presented in (9) is used [20].

$$S = \sqrt{\sum_{s=1}^{h} \frac{\left(R_s - \hat{R}_s\right)^2}{h-1}} \tag{9}$$

The determination of the unilateral confidence limits, both upper and lower, is determined by (10) and (11) respectively. Where g is the critical value of the "t" distribution with a significance level of 5% . This significance level determines whether the result is considered statistically significant [21].

$$\text{upper unilateral limit} = \hat{R}_s + g \cdot S \tag{10}$$

$$\text{lower unilateral limit} = \hat{R}_s - g \cdot S \tag{11}$$

D. Fault Identification Using Neural Networks

The technique for identifying faults in the PV through variation of R_s is performed using neural networks. The training of the neural network requires multiple data points at different operating conditions, corresponding to the inputs G and $\hat{R}_s$. The neural network used is a MLP trained by supervised learning, considering its outputs as: normal operation $[1\ 0\ 0]$, failure 1 due to mismatch $[0\ 1\ 0]$ and failure 2 due to humidity degradation $[0\ 0\ 1]$. The database was obtained from the page of the Tungurahua hydrometeorological network [22], where there are different sections of weather stations, including the Ambato Family Park, located in Ecuador, province of Tungurahua, with coordinates latitude -1.2439 and longitude -78.6611, which has the parameters of ambient temperature [°C] and solar radiation $[W/m^2]$, which were used for the inputs of the estimation and identification models by neural networks.

For the preprocessing of the obtained database, six months of data were used (from October 10, 2022 to April 10, 2023), which were processed to take data every 5 minutes for a total of 52,704.00 data. During the time of data collection, we collected information of failures which were generated by different types of random failures caused by changes in the internal resistance. After data acquisition, a total of 52,704.00 data were obtained, where: 64% of the database (33,730.56 data) are used for training, 18% (9,486.72 data) for testing and 18% (9,486.72 data) for model validation, the same that were randomly distributed.

Several NN architectures are trained and sensitivity analysis is used, obtaining the MLP shown in Fig. 4 as the most optimal NN. This NN consists of three layers. The input layer comprises two neurons corresponding to irradiation G and estimated series resistance $\hat{R}_s$. The hidden layer consists of 10 neurons, which are connected to the input layer through synaptic weights w_{ij}. Each neuron has a bias θ with a value of zero. The selected activation function f'_j is hyperbolic tangent (tanh) due to its non-linearity and convergence towards better learning. Finally, the output layer consists of three neurons representing normal operation NOP, Fault 1 (F1), and Fault 2 (F2). The output neurons are connected to the hidden layer through synaptic weights w'_{jz}, and the chosen activation function f'_z is sigmoid, which allows for binary classification. Each output neuron has its respective bias θ. The outputs of the neural network are described in Table I, including the causes, effects, and power behavior at the PV

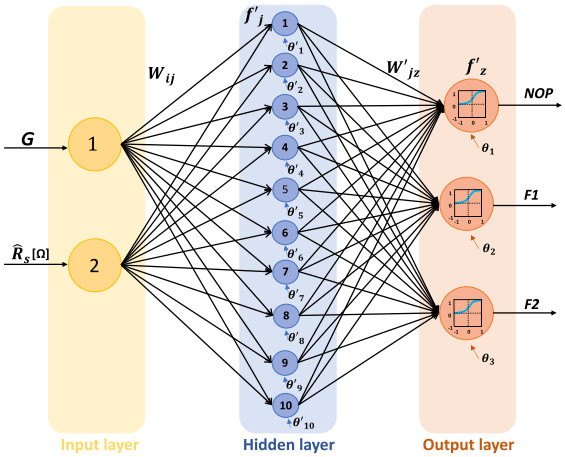

Fig 4. MLP neural network structure for fault identification.

TABLE I. SERIES RESISTANCE FAULTS AND NEURAL NETWORK OUTPUT.

Faults	Cause	(↑)Increase (↓) Decrease of R_s value	Effect	Neural network output
Normal Operation	None	None	None	$[1\ 0\ 0]$
Fault 1	Mismatch Failures	$R_s\ [\Omega]\ \uparrow$	Power Loss	$[0\ 1\ 0]$
Fault 2	Moisture Degradation	$R_s\ [\Omega]\ \downarrow$	Power Increase	$[0\ 0\ 1]$

V. Results

This section presents and analyzes the results obtained from evaluating the series resistance estimator $\hat{R}_s$ and the performance of the fault identification system. The case study focuses on the PV model Du Pont Apollo DA130-C2 implemented in Matlab/Simulink software, with the characteristics described in Table II.

TABLE II. PANEL PROPERTIES DU PONT APOLLO DA130-C2

Description	Parameters	Value
Nominal power output	P_{pv}	130 [W]
Environment Temperature	T_o	25° [C]
Short circuit current	I_{sc}	1.28 [A]
Open circuit voltage	V_{oc}	154.96 [V]
Series resistor	R_s	15.1879 [Ω]
Shunt resistor	R_{sh}	807.101 [Ω]

An irradiance profile is used which is described in section 4.2. The irradiance profile corresponds to the validation set, to February 5, 2023, see Figure 5(a), where the

maximum irradiance point is $850\ [W/m^2]$ at 12 o'clock on the same day. For the analysis, 24 operating points are used, which are average values representing one hour, see Figure 5(b).

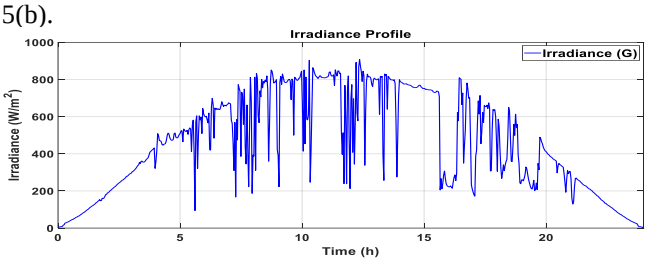

a)

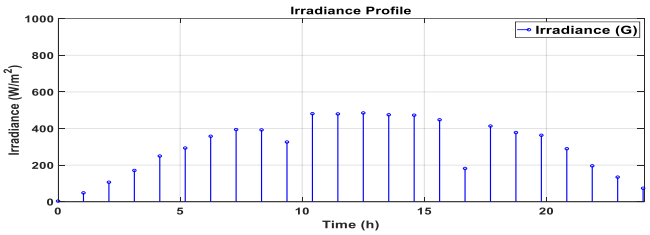

b)

Fig. 5. Irradiance profile, a) Daily irradiance and b) Irradiance representation in hours.

A. *Evaluation of the Resistance Estimator*

The series resistance is internally located in the PV panel and cannot be directly measured. However, through simulation, this change can be implemented within the PV model by emulating different values of R_s, with this information, the performance of the proposed estimator can be validated. The estimated value should fall within a $\pm 5\%$ confidence Interval, as presented in section IV-(A). First, the evaluation is conducted under NOP conditions (see Fig. 6.), where the estimated resistance values (black circles) are found around the actual operating resistance value (green line) provided by the manufacturer, which is $15.1879\ [\Omega]$. It can be verified that the estimation at all operating points, under different irradiance profiles, adheres to the confidence band. In other words, the estimated resistance does not exceed the upper confidence interval of $15.45\ [\Omega]$ (red line) or the lower confidence interval of $15.19\ [\Omega]$ (dashed red line).

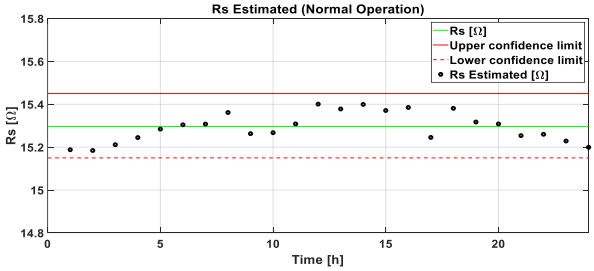

Fig. 6. Estimated resistance in normal operation.

In the Fig. 7. shows the validation of the estimator at different values of R_s. In the interval $(0-6h)$, the R_s value remains constant at the one defined by the manufacturer, which corresponds to the NOP condition. The estimated value falls within the confidence band. Then, in the time interval $(7-12h)$, the series resistance value is increased $R_s = 20\ [\Omega]$, and once again, the estimated value remains within the confidence intervals. Finally, in the interval $(20-24\,h)$, the series resistance value is decreased $R_s = 10\ [\Omega]$, and it is observed that the estimated value still falls within the confidence band.

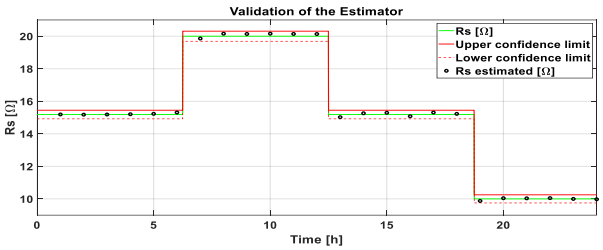

Fig. 7. Validation of the estimator at different values of R_s.

B. *Failure Identification System Evaluation*

In Fig. 8, the response obtained at the output of the identifier is shown when applying two inputs. The first input corresponds to the radiation profile Fig. 5(b), and the second input is the estimated resistance shown in Fig. 6. As deduced earlier, the estimator provides the estimated series resistance $\hat{R}_s$ for the normal operating mode, respecting the confidence intervals. Therefore, the good performance of the estimator is validated because the output of the identifier shows the normal operating mode, indicated by the reading of $[0.95 \quad 0.025 \quad 0.025]$, which are interpreted as follows: If $Out < 0.5$ it is equivalent to 0, while if $Out \geq 0.5$ it is 1, therefore the output of the neural network is $[1 \quad 0 \quad 0]$.

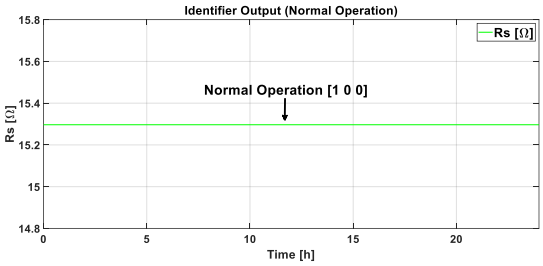

Fig. 8. Output response of the identifier in normal operation (NOP).

C. *Evaluation of the Identification System in Different Fault Scenarios*

Next, the identifier is evaluated against the radiation operating points shown in Fig. 5(b), with the input of estimated resistance from Fig. 6. As can be shown in Fig 9, in the interval $(0-6h)$ and $(12-18h)$, as expected, the estimated resistance corresponds to the normal operating condition, and the estimator correctly outputs $[1 \quad 0 \quad 0]$, which represents NOP. In the interval $(6-12h)$, the network output is $[0 \quad 0 \quad 1]$, indicating Fault 2. Finally, in the interval $(19-24h)$, the resistance decreases significantly due to Fault 1, and the output is $[0 \quad 1 \quad 0]$, validating the correct identification of faults at different operating points.

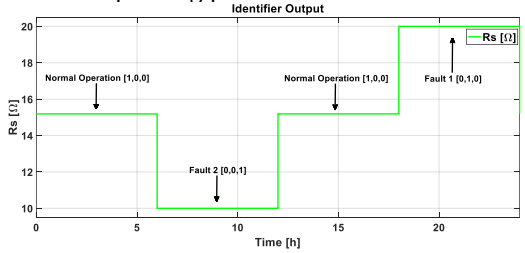

Fig. 9. Identification of failures at different values of R_s.

In Fig. 10 shows the effects of the faults caused by the variation of the resistance on the output power of the panel

(red color) with respect to the power obtained in normal operation (blue color). In the range (0 – 6h) and (12 – 18h) the power is the expected in normal operation, therefore the graphs are superimposed, in the range (6 – 12h) it is observed the fault 2 caused by the degradation due to humidity which causes an increase of the power and in range (19 – 24h) it can be observed that the power decreases due to fault 1 which is caused by mismatch.

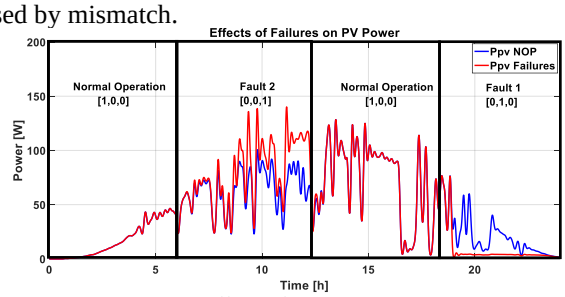

Fig. 10. Effects of Failures on PV power.

In Fig. 11, the impact of faults on PV power is depicted. The curve (blue color) represents normal operating conditions, while the curve (red color) represents the effects of shading faults, which result in power loss. On the other hand, the curve (green color) represents the effects of Fault 2, specifically moisture degradation, where power is increased. This indicates the occurrence of hotspots on the panel, leading to damage.

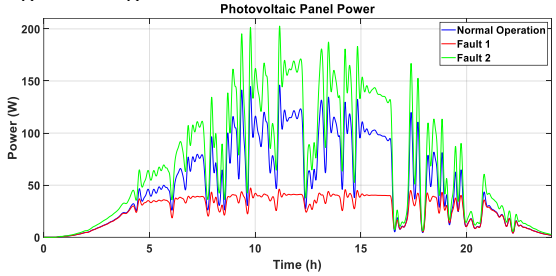

Fig. 11. Effects of faults on photovoltaic panel power.

VI. Conclusions

The system proves to be efficient in identifying faults, as it correctly identifies all faults in 9,486.72 operating points tested under different irradiance profiles. Tests are conducted using PV from various manufacturers, demonstrating its compatibility and ability to integrate with any system. The fault identification system is capable of distinguishing between power changes in the PV caused by variations in irradiance and those caused by faults, thanks to the training of the MLP. This prevents confusion when identifying the type of fault. Additionally, the recursive least squares technique with a forgetting factor, including confidence intervals, ensures efficient fault identification. The estimator has shown high reliability, guaranteeing a 95% confidence level in the estimation. It also demonstrates adaptability to changes in the PV and continuous updating of the estimation. Future work will expand the number of failures to be detected.

VII. Acknowledgments

This work was supported in part by the Universidad de las Fuerzas Armadas ESPE through the Project “Optimal energy management systems for hybrid generation systems”, under Project 2023-pis-03.

References

[1] J. Peng, L. Lu, y H. Yang, «Review on life cycle assessment of energy payback and greenhouse gas emission of solar photovoltaic systems», *Renew. Sustain. Energy Rev.*, vol. 19, pp. 255-274, mar. 2013, doi: 10.1016/j.rser.2012.11.035.

[2] V. Moutinho y M. Robaina, «Is the share of renewable energy sources determining the CO2 kWh and income relation in electricity generation?», *Renew. Sustain. Energy Rev.*, vol. 65, pp. 902-914, nov. 2016, doi: 10.1016/j.rser.2016.07.007.

[3] A. P. Moya, P. J. Pazmiño, J. R. Llanos, D. Ortiz-Villalba, y C. Burgos, «Distributed Secondary Control for Battery Management in a DC Microgrid», *Energies*, vol. 15, n.º 22, p. 8769, 2022.

[4] N. Kannan y D. Vakeesan, «Solar energy for future world: - A review», *Renew. Sustain. Energy Rev.*, vol. 62, pp. 1092-1105, sep. 2016, doi: 10.1016/j.rser.2016.05.022.

[5] M. Santhakumari y N. Sagar, «A review of the environmental factors degrading the performance of silicon wafer-based photovoltaic modules: Failure detection methods and essential mitigation techniques», *Renew. Sustain. Energy Rev.*, vol. 110, pp. 83-100, 2019.

[6] A. Tabanjat, M. Becherif, y D. Hissel, «Reconfiguration solution for shaded PV panels using switching control», *Renew. Energy*, vol. 82, pp. 4-13, 2015.

[7] Z. Meng, Y. Zhao, S. Tang, y Y. Sun, «An efficient datasheet-based parameters extraction method for two-diode photovoltaic cell and cells model», *Renew. Energy*, vol. 153, pp. 1174-1182, 2020.

[8] M. H. Ali, A. Rabhi, A. El Hajjaji, y G. M. Tina, «Real time fault detection in photovoltaic systems», *Energy Procedia*, vol. 111, pp. 914-923, 2017.

[9] H. Taud y J. F. Mas, «Multilayer perceptron (MLP)», *Geomat. Approaches Model. Land Change Scenar.*, pp. 451-455, 2018.

[10] A. Hichri *et al.*, «Genetic-Algorithm-Based Neural Network for Fault Detection and Diagnosis: Application to Grid-Connected Photovoltaic Systems», *Sustainability*, vol. 14, n.º 17, Art. n.º 17, ene. 2022, doi: 10.3390/su141710518.

[11] J.-S. Jeong, N. Park, y C. Han, «Field failure mechanism study of solder interconnection for crystalline silicon photovoltaic module», *Microelectron. Reliab.*, vol. 52, n.º 9, pp. 2326-2330, sep. 2012, doi: 10.1016/j.microrel.2012.06.027.

[12] R. G. Vieira, M. Dhimish, F. M. U. de Araújo, y M. I. da Silva Guerra, «Comparing multilayer perceptron and probabilistic neural network for PV systems fault detection», *Expert Syst. Appl.*, vol. 201, p. 117248, sep. 2022, doi: 10.1016/j.eswa.2022.117248.

[13] Y. Xu, W. Jin, y X. Zhu, «Parameter identification of photovoltaic cell based on improved recursive least square method», en *2017 20th international conference on electrical machines and systems (ICEMS)*, IEEE, 2017, pp. 1-5.

[14] A. Haque, K. V. S. Bharath, M. A. Khan, I. Khan, y Z. A. Jaffery, «Fault diagnosis of photovoltaic modules», *Energy Sci. Eng.*, vol. 7, n.º 3, pp. 622-644, 2019.

[15] A. Triki-Lahiani, A. B.-B. Abdelghani, y I. Slama-Belkhodja, «Fault detection and monitoring systems for photovoltaic installations: A review», *Renew. Sustain. Energy Rev.*, vol. 82, pp. 2680-2692, 2018.

[16] N. Gokmen, E. Karatepe, S. Silvestre, B. Celik, y P. Ortega, «An efficient fault diagnosis method for PV systems based on operating voltage-window», *Energy Convers. Manag.*, vol. 73, pp. 350-360, 2013.

[17] S. Silvestre, A. Chouder, y E. Karatepe, «Automatic fault detection in grid connected PV systems», *Sol. Energy*, vol. 94, pp. 119-127, 2013.

[18] A. L. Bruce, A. Goel, y D. S. Bernstein, «Convergence and consistency of recursive least squares with variable-rate forgetting», *Automatica*, vol. 119, p. 109052, 2020.

[19] W. Xiao, M. G. Lind, W. G. Dunford, y A. Capel, «Real-time identification of optimal operating points in photovoltaic power systems», *IEEE Trans. Ind. Electron.*, vol. 53, n.º 4, pp. 1017-1026, 2006.

[20] R. E. Walpole, R. H. Myers, y S. L. Myers, *Probabilidad y estadística para ingenieros*. Pearson Educación, 1999.

[21] José Olmedo Morán y Patricio Bracero Lara, «BOLETIN CLIMATOLOGICO SEMESTRAL 2016», *INAMHI*, n.º 001, p. 26.